Isothermal Thickening and Thinning Processes in Low Molecular Weight Poly(ethylene oxide) Fractions Crystallized from the Melt. 4. End-Group Dependence

Stephen Z. D. Cheng,* Scott S. Wu, Jianhua Chen, Qizhuo Zhuo, and Roderic P. Quirk

Institute and Department of Polymer Science, The University of Akron, Akron, Ohio 44325-3909

Ernst D. von Meerwall

Physics Department, The University of Akron, Akron, Ohio 44325

Benjamin S. Hsiao

Fiber Division, Experimental Station, E.I. du Pont de Nemours and Company, Wilmington, Delaware 19880-0302

Anton Habenschuss and Paul R. Zschack

Oak Ridge National Laboratory, Oak Ridge, Tennessee 37831

Received January 25, 1993; Revised Manuscript Received June 22, 1993•

ABSTRACT: A series of low molecular weight poly(ethylene oxide) (PEO) fractions with different molecular weights (MW=3000 and 7100) and end groups (–OH, $-OCH_3$, $-OC(CH_3)_3$, and $-OC_6H_5$) have been systematically studied. The end-group effect on diffusional motion in the melt of these PEO fractions was characterized by self-diffusion coefficient measurements through nuclear magnetic resonance. Wide-angle X-ray diffraction experiments indicated that the crystal structures of the PEO fractions with different end groups were identical during and after crystallization. The existence of nonintegral folding chain (NIF) crystals in these PEO fractions in a wide undercooling region was observed by time-resolved synchrotron small-angle X-ray scattering, differential scanning calorimetry, and transmission electron microscopy experiments. The integral folding chain (IF) crystals were found to be formed through both thickening and thinning processes during and/or after the NIF crystallization. It was also found that, with increasing molecular weight and size of the end group, the thickening and thinning processes were increasingly hampered. Of additional interest, the fold length of initial NIF crystals not only increases with crystallization temperature (or decreasing undercooling) for each PEO fraction as commonly observed in polymer lamellar crystals but also changes with the size of the end group. The kinetics of transformation from NIF to IF crystals is explained through the chain sliding diffusional motion along the direction perpendicular to the lamellar surface, which is end-group size dependent. Linear crystal growth rate data measured via polarized light microscopy confirmed that the existence of bulky end groups reduces NIF crystal growth rates for PEO (MW = 3000) fractions. With increasing molecular weight, the end-group dependence gradually vanishes due to the introduction of chain entanglement.

Introduction

In the previous publications of this series,[1-3] it has been recognized that, during crystallization of low molecular weight poly(ethylene oxide) (PEO) fractions, a nonintegral folding chain (NIF) crystal forms initially and integral chain (IF) crystals are subsequently developed via thickening and/or thinning processes. This NIF behavior in *n*-alkanes has been first reported by Ungar and Keller[4,5] in the melt crystallization and later by Organ, Ungar, and Keller[6] for solution crystallization. The NIF crystal in PEO fractions has been observed not only between the extended chain [IF(n=0)] and the once-folded chain [IF-(n=1)] crystals[1] but also between the IF crystals involving more than one fold.[2] The thickening and thinning results have been explained through thermodynamic and kinetic reasoning. In addition, the fold length of initial NIF crystals was found to increase with decreasing undercooling ($\Delta T = T_m - T_c$, where T_m is the thermodynamic melting temperature and T_c is the crystallization temperature) as commonly observed in polymer lamellar crystals. With increasing molecular weight and the number of folds, the thickening and thinning processes are increasingly hampered. Only at sufficient high molecular weights may the NIF crystal be permanently retained. As a result, a continuous increase in the fold length of NIF lamellar crystals with decreasing undercooling has been observed during polymer crystallization.[3]

In the late 1960s, Arlie, Spegt, and Skoulios have reported small-angle X-ray scattering (SAXS) results on low molecular weight PEO, which showed that the long period increased stepwise with temperature.[7-9] In the early 1970s, the observation of unique IF crystals in these PEO fractions was made by Kovacs et al.,[10-16] whose results were initially explained by invoking hydroxy end groups (–OH) as a possible network of hydrogen bonding on IF crystal surfaces. This concept led to research interest in the study of end-group dependence in crystallization and crystal melting behavior of low molecular weight PEO fractions. Booth et al.[17-20] have first investigated low molecular weight PEO fractions with different end groups, including alkoxy[17,18] and acetoxy end groups,[19] Kovacs et al. have also reported a PEO fraction with diphenyl and hydroxy end groups.[13] All of these PEO fractions exhibit similar IF crystals grown from the metal. Since these end groups differ from each other by their functionality and size, a specific role to hydrogen-bonding interactions

* To whom the correspondence should be addressed.
• Abstract published in *Advance ACS Abstracts*, August 15, 1993.

0024-9297/93/2226-5105$04.00/0 © 1993 American Chemical Society

involving hydroxy end groups is not expected in the IF crystal formation.[20] Shimada et al. found that low molecular weight PEO fractions with phenyl end groups do not show a stepwise increase in crystal lamellar thickness grown from the melt.[21] Similar behavior in PEOs with other bulkier end groups were also reported.[22-24] Recently, we have investigated one PEO fraction with methoxy end groups ($-OCH_3$) (MPEO)[25] and observed that the IF crystal was actually formed via a transformation of NIF crystals. The thickening and thinning processes in this transformation were faster compared to the PEO fraction with the same molecular weight and hydroxy end groups.

In this paper, we have systematically studied the end-group dependence of low molecular weight PEO fractions on crystallization behavior. Two different molecular weights of PEO fractions having four different end groups have been investigated. In particular, the roles of different end groups affecting NIF crystal formation kinetics, thickening and thinning processes, and lamellar crystal morphology are discussed.

Experimental Section

Materials. Two low molecular weight PEO fractions with MW = 3000 and 7100 were purchased from Polymer Laboratories, Ltd., as control materials, which have been further refractionated in our laboratory. The polydispersities are 1.02 and 1.04, respectively. These PEO fractions possess hydroxy end groups (-OH). The PEO fractions were also methoxylated, *tert*-butoxylated, and phenoxylated. The chemical procedure involved ditosylate of PEO fractions (DTP) as intermediates, which is formed in the reaction of PEO fractions with *p*-toluenesulfonyl chloride in 4-(dimethylamino)pyridine, triethylamine, and dichloromethane at room temperature for 24 h according to the method proposed by Devos and Goethals:[26] The synthesis of methoxy-

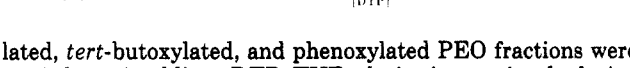

lated, *tert*-butoxylated, and phenoxylated PEO fractions were carried out via adding a DTP–THF solution into a stirred solution of sodium methoxide, sodium *tert*-butoxide, or sodium phenoxide in THF, correspondingly. The reactions were at 65 °C for 16 h,

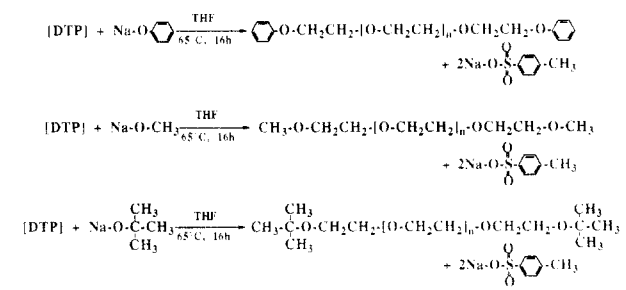

and the mixtures were kept under an argon atmosphere with stirring. The precipitates were filtered, dried, and redissolved into CH_2Cl_2. The insoluble impurities were eliminated by filtration. The second precipitates were obtained from a CH_2Cl_2 solution by adding ether and refiltered. The filtered products were then dissolved in absolute ethanol at 60 °C and gently cooled to −18 °C for recrystallization. The above purification procedure was repeated eight times. Further purification was carried out by column chromatography in a silica gel column using CH_2Cl_2 as the eluting solvent.

In order to distinguish the different end groups in PEO fractions, the PEO fractions with hydroxy end groups are abbreviated as HPEO, those with methoxy end groups, MPEO, those with *tert*-butoxy end groups, TPEO, and those with phenoxy end groups, PPEO.

Proton ^1H solution nuclear magnetic resonance (NMR), infrared spectroscopy (FTIR), and ultraviolet spectroscopy (UV) were used to detect the unreacted hydroxy end groups.[27] In all cases, no -OH residual trace was found. The gel permeation chromatography (GPC) data for these samples are listed in Table I.

Table I. Molecular Parameters of PEO Fractions with Different End Groups

fractions	M_n ($\times 10^3$)	M_w/M_n	av length (nm)	$T_m(n=0)$ (°C)
		MW = 3000		
HPEO	2.90	1.02	18.9	58.7
MPEO	2.95	1.02	19.2	59.3
PPEO	3.05	1.02	20.1	58.1
TPEO	3.01	1.02	19.5	58.6
		MW = 7100		
HPEO	7.10	1.04	44.9	64.0
MPEO	7.15	1.04	45.2	64.2
PPEO	7.25	1.04	46.1	63.8

Instrument and Experiments. Differential scanning calorimetry (DSC) experiments were conducted on a Seiko DSC 220. A typical sample weight ranging from 0.1 to 1 mg was used, depending upon the heating rate. The pan weights were kept constant with an accuracy of ±0.001 mg. The temperature and heat flow of DSC were carefully calibrated by standards. Isothermal experiments were carried out by quenching the samples from the isotropic melt to desired crystallization temperatures in order to record exothermic crystallization processes. The samples were then heated to above their melting temperatures without prior cooling. A standard heating rate of 5 °C/min was used unless otherwise indicated.

Time-resolved synchrotron small-angle X-ray scattering (SAXS) experiments were carried out at the Oak Ridge National Laboratory beam line X-14 at the National Synchrotron Light Source (NSLS). The X-ray wavelength was 0.154 98 nm (8.000 keV). The X-ray beam was focused at the sample position through a dynamically bent Si crystal monochromator with a beam size of 0.1 × 1.0 mm (V × H). A position-sensitive proportional counter (Ordella 1020) was used to record the scattering patterns. A customized temperature-jump hot stage was built and situated on a Huber goniometer for isothermal measurements. The temperature of this hot stage was calibrated with standard materials during the beam radiation. The precision of the temperature controller was ±0.5 °C. Detailed equipment setup was published in a previous publication.[1] The Lorentz correction was made by multiplying the intensity, I (counts per second), with s^2 ($s = 2 \sin\theta/\lambda$ with λ as the wavelength of the synchrotron X-ray radiation).

Wide-angle X-ray diffraction (WAXD) experiments were carried out through a Rigaku 12-kW rotating-anode generator coupled with a diffractometer. A temperature cell was equipped on the WAXD equipment and had an accuracy of ±0.5 °C. Isothermal crystallization of PEO fractions was conducted to record time-resolved crystallinity developments. The monochromatized X-ray beam from Cu Kα radiation with a wavelength of 0.154 38 nm was used in this measurement.

Self-diffusion coefficients of these PEO fractions in the melt were determined by a pulsed-gradient spin-echo (PGSE) nuclear magnetic resonance (NMR) method.[28] A detailed description of the experiments can be found in a previous publication.[29] In brief, we measured the proton NMR at 33 MHz using a spin-lock CPS-2 spectrometer with a Varian high-impedance current-regulated electromagnet. The principle echo on-resonance without Fourier transform (FT) was measured using radio-frequency phase-sensitive detection. Its attenuation in the presence of a pair of applied magnetic field gradient pulses was also detected. For all samples, measurements at three temperatures (70.5, 80.5, and 90.5 °C) were conducted. To obtain accurate data for self-diffusion coefficients, we have incorporated the effect of polydispersity using a model of molecular weight averages M_n and M_w and molecular weight distribution (which has been found to closely resemble a log-normal distribution).[30] In addition, information about the PEO critical molecular weight M_c, at which entangled behavior is first observed in a monodisperse melt, was also estimated (M_c=4400) using Ferry's compilation. The number-average molecular weight of entanglement in PEO fractions has been estimated to be about 7000–8000.[29,31]

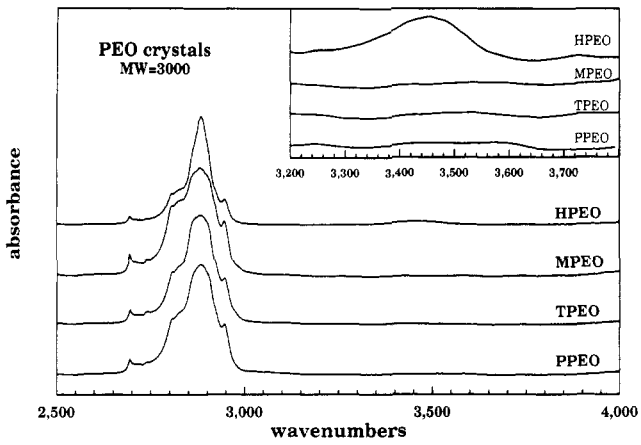

Figure 1. FTIR spectra of four PEO(MW=3000) fractions with different end groups at room temperature.

Infrared spectroscopy (FTIR) measurements were performed through a Mattson Galaxy 5020. In order to determine the nature of the end groups, particular interest was taken in the spectrum ranging between 2500 and 4000 cm^{-1}, which represents hydrogen-bonding and O–H stretching vibrational modes. A temperature unit was added to the equipment to detect the hydrogen-bonding change with temperature and the phase transition.

Finally, polarized light microscopy (PLM) experiments were conducted through an Olympus HB-2 microscope equipped with a Mettler FP-82 hot stage. The PEO samples were prepared in between two thin glass slides in a nitrogen atmosphere. Isothermal experiments followed the exact procedure as reported before.[32] The linear crystal growth rate data were measured from the spherulitic or the hedritic growth of the PEO crystals. Transmission electron microscopy (TEM) observations were also made to determine the lamellar thickness. For TEM measurements, the PEO fraction samples were isothermally crystallized as in other experiments. The samples were coated by heavy metal (Au/Pt 0.4/0.6) and carbon and were subsequently dissolved in water. The replicas were then recovered in acetone. A JEOL JEM-120U TEM with an accelerating voltage of 100 kV was used.

Results

Characterizations of the End Groups in PEO Fractions. In order to investigate the effect of end groups, FTIR experiments were used to detect the hydrogen-bonding and O–H stretching vibrations in the solid state. The results are shown in Figure 1. The PEO fractions with a MW = 3000 are used in this study, which has the highest end-group density and, therefore, should illustrate the largest difference in the spectra if there is a polarized vibrational mode change. For the HPEO fraction (with –OH end groups) a broad vibrational band around 3500 cm^{-1} is observed. This is characteristic of the existence of hydrogen bonding and O–H stretching. Nevertheless, the spectra of three other PEO fractions with $-OCH_3$, $-OC(CH_3)_3$, and $-OC_6H_5$ do not exhibit such a band. When the HPEO fraction is heated to above its melting temperature, it still exhibits a strong absorption band around 3500 cm^{-1} with a relatively narrow absorption peak compared with that in the solid state, as shown in Figure 2.

Figure 3 shows the powder WAXD patterns for four PEO fractions (HPEO, MPEO, TPEO, and PPEO) with a MW = 3000 after the samples were annealed at 45 °C for 48 h. For comparison, WAXD patterns of the same fractions quenched from the melt are also included in this figure. It is found that the diffraction peak positions are similar for different samples prepared at differnt conditions, which indicates that the crystal structures (monoclinic) in these fractions are essentially unchanged with different end groups and crystallization conditions. All

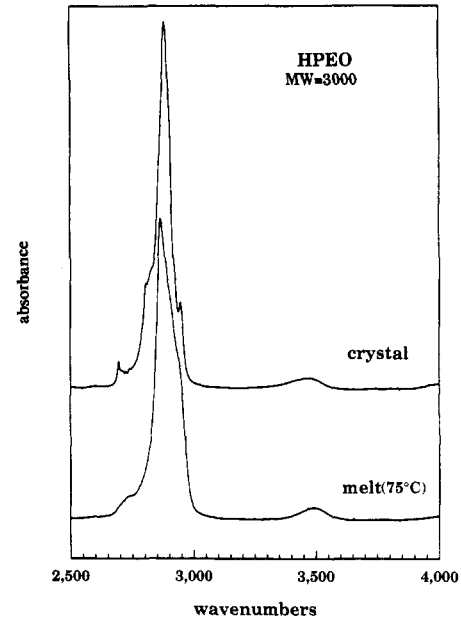

Figure 2. FTIR spectra of the HPEO(MW=3000) fraction with hydroxy end groups in the melt and solid state.

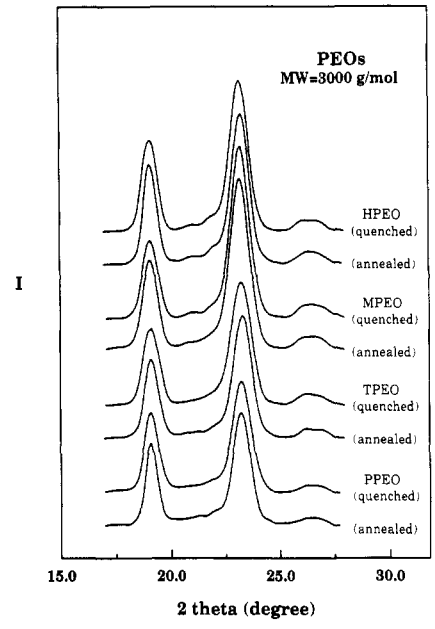

Figure 3. WAXD powder patterns of four PEO (MW=3000) fractions with different end groups after the samples were quenched to 30 °C and annealed at 45 °C for 48 h.

PEO fraction samples show high degrees of (weight fraction) crystallinity above 90% in these diffraction patterns. Since the end-group density decreases with increasing molecular weight, we find that those three PEO fractions with a MW = 7100 listed in Table I also possess the same crystal structure.

To understand the crystallization behavior of these PEO fractions with different end groups, it is helpful to know the diffusional motion of these PEO fractions in the melt. This can be achieved by the self-diffusion coefficient (D) measurements through NMR. Parts a and b of Figure 4 show the relationships between logarithmic self-diffusion coefficients ($\log D$) of these PEO fractions having different end groups and reciprocal temperatures measured for two different molecular weights (MW=3000 and 7100). It is apparent that, for each fraction, the self-diffusion coefficient decreases with increasing temperature. From Figure 4a, the MPEO fraction possesses the highest self-diffusion coefficients among these PEO(MW=3000) frac-

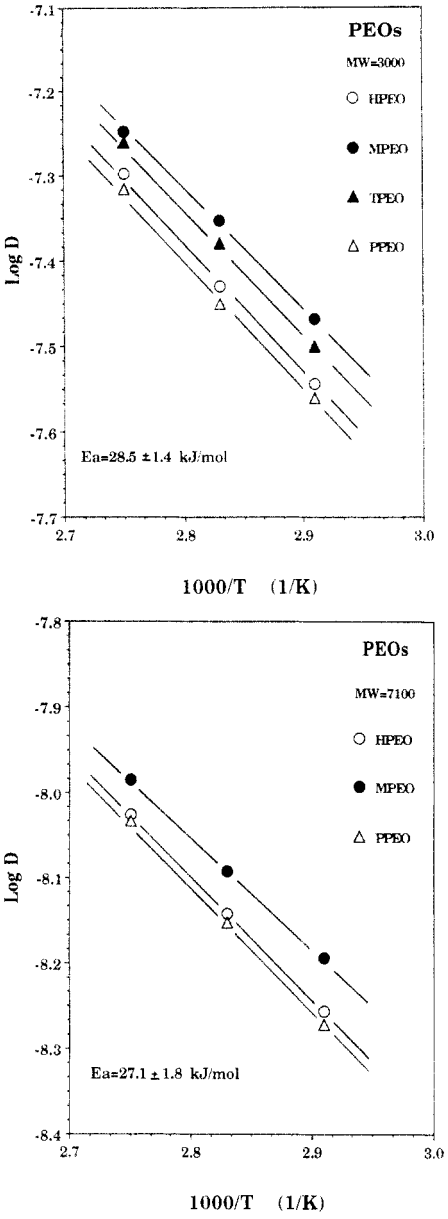

Figure 4. Relationships between the logarithmic self-diffusion coefficient and reciprocal temperature for PEO fractions with different end groups: (a) MW = 3000; (b) MW = 7100.

tions. It is followed by TPEO, HPEO, and finally PPEO fractions. The slope of each PEO fraction is proportional to the activation energy of the diffusional motion, and their activation energies calculated are very close to each other as 28.5 ± 1.4 kJ/mol. When the molecular weight increases to 7100, the self-diffusion coefficient of the MPEO fraction is still faster than the other two (HPEO and PPEO) fractions, while the HPEO and PPEO fractions show very closed log D values. The activation energy slightly decreases to 27.1 ± 1.8 kJ/mol for the PEO fractions with a MW = 7100.

Crystallization and Crystal Melting of the PEO Fractions. Figure 5 shows a set of isothermal (43 °C) DSC exothermic traces for PEO(MW=3000) fractions with different end groups. It is seen that the overall crystallization rate changes with different end groups. The rate of the MPEO fraction is fastest (time=8 min), followed by HPEO (20 min), TPEO (30 min), and, finally, PPEO (70 min). The definition of the total crystallization for these fractions is that the exothermic process is ended and the heat of crystallization is near the equilibrium value in DSC or the maximum crystallinity is reached by WAXD measurements (see below). In addition, multiple exo-

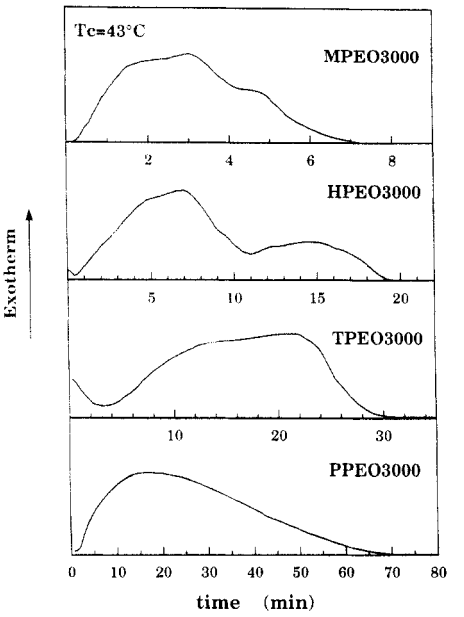

Figure 5. DSC exothermic isothermal traces for four PEO fractions with MW = 3000 crystallized at 43 °C.

thermic peaks were observed in HPEO, MPEO, and TPEO fractions, while only a single exothermic peak is found in PPEO fractions. The multiple exothermic peaks were deconvoluted using the method previously described.[33]

A parallel study by time-resolved WAXD experiments is illustrated in Figure 6, where HPEO (Figure 6a), MPEO (Figure 6b), PPEO (Figure 6c), and TPEO (Figure 6d) crystallization kinetics are shown at the crystallization temperature of 43 °C. A gradual development of the crystallinity in these fractions is seen. The maximum degree of crystallinity of the PPEO fraction is achived after 70 min, while for the TPEO fraction only 30 min is needed. In these two fractions, only an initial stage of crystallization is shown in Figure 6c,d to indicate the crystallinity changes with time. Prolonged experiments were conducted to confirm the completion of crystallization. In Figure 6a,b, HPEO and MPEO fractions are found to crystallize faster than PPEO and TPEO fractions. In general, the increase of crystallinity is approximately monotonous, while no decrease of the diffraction intensity with time is found in all the cases studied.

Crystal melting behavior of these fractions is studied, and Figure 7 shows, as an example, a set of DSC heating traces for the PPEO(MW=3000) fraction. It is apparent that the low melting peak is a main contributor to the heat of fusion in a crystallization temperature range below 46 °C, and its peak temperature is undercooling-dependent (a very small shoulder appearing below 40 °C can also be seen). Only at crystallization temperatures above 46 °C does a high melting peak start to develop. This peak increases its share of the total heat of fusion with the increasing temperature. Above T_c = 46 °C, the low melting peak becomes less undercooling-dependent and decreases at high crystallization temperature. In contrast, the high melting peak also slightly increases with crystallization temperature without reaching a constant melting temperature at the highest crystallization temperature region as observed in the HPEO and MPEO fraction cases.[25,33] Figure 8 illustrates the relationships between melting temperature (T_m) and crystallization temperature (T_c) for both PPEO and TPEO fractions with MW = 3000. For HPEO and MPEO fractions with the same molecular weight, the T_m-T_c relationships have been published previously.[25,33] In this figure, it is seen that for TPEO-

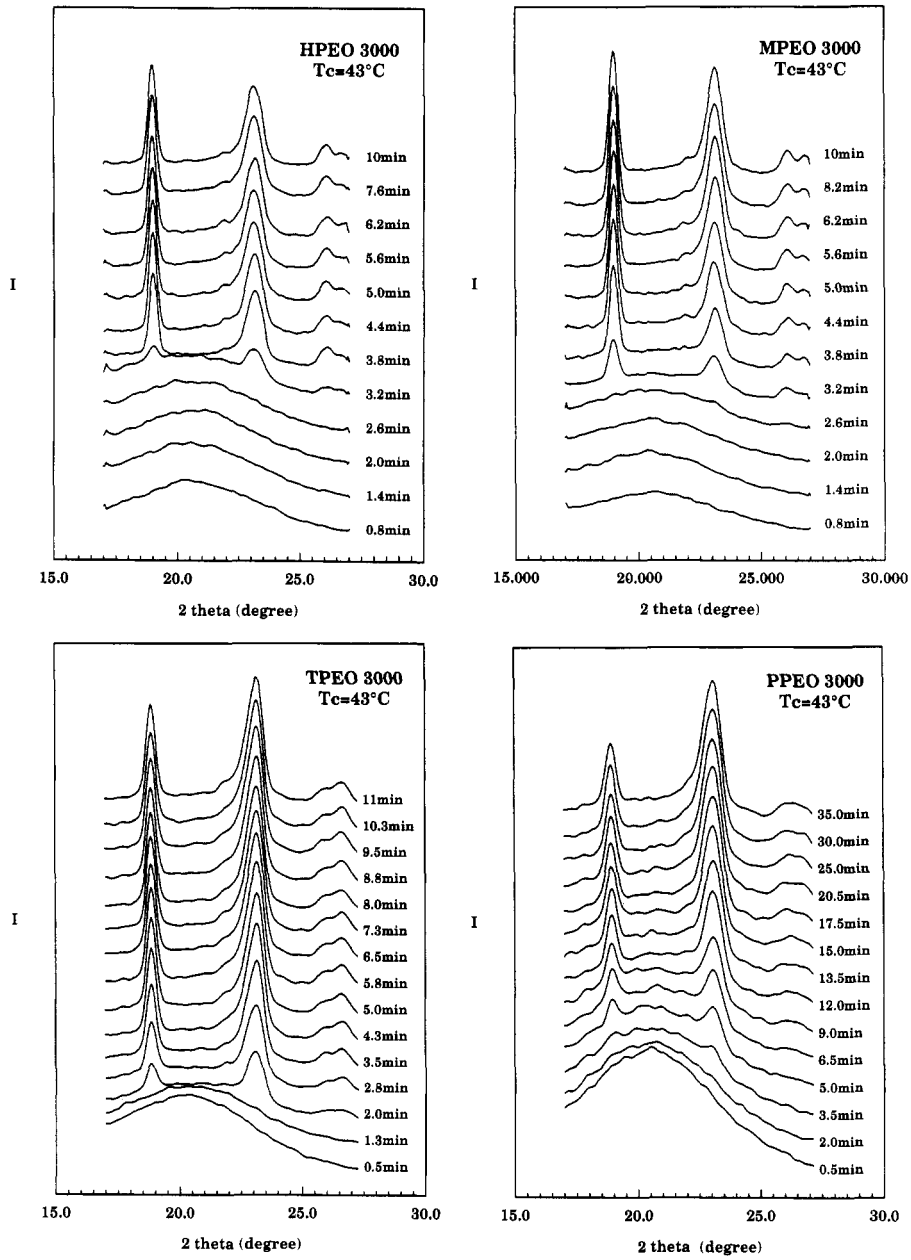

Figure 6. WAXD patterns for four PEO(MW=3000) fractions isothermally crystallized at 43 °C at different times: (a) HPEO, (b) MPEO, (c) PPEO, and (d) TPEO.

(MW=3000) two endothermic peaks appear even at T_c = 40 °C. The lower peak is undercooling-dependent, while the middle peak is less undercooling-dependent, which may be attributed to the melting of IF(n=1) crystals. Above T_c = 45 °C, only one high melting endotherm can be observed. The extrapolations of the high melting temperatures intercepting the $T_m = T_c$ line yield the IF(n=0) crystal melting temperatures. The results are 58.1 °C for PPEO(MW=3000) and 58.6 °C for TPEO(MW=3000). Compared to the IF(n=0) crystal melting temperatures of 58.7 °C for HPEO(MW=3000)[25] and 59.3 °C for MPEO-(MW=3000),[33] the IF(n=0) crystal melting temperatures for the fractions with different end groups are within 1.5 °C from one another. In the MPEO(MW=7100) fraction, the crystal melting behavior is similar to its counterpart HPEO.[2] Nevertheless, the PPEO(MW=7100) fraction shows a much straightforward crystal melting behavior compared with the other two fractions. Figure 9 shows such behavior of PPEO(MW=7100). Below T_c = 51 °C, only one undercooling-dependent endothermic peak exists with a continuously increasing position. The second melting peak was observed only at T_c above 55 °C.

Finally, Figure 10 shows DSC endothermic melting traces of the PPEO(MW=3000) fraction crystallized at 44 °C for different times. After 250 min the overall crystallization ends. The heat of fusion approaches 7.10 kJ/mol, which is equivalent to a 90% degree of crystallinity. Only one melting endothermic peak is observed (top scan in Figure 10). Further annealing at 44 °C for longer time shows little increase in the overall heat of fusion but a formation of the higher crystal melting temperature around 56–57 °C which is representative of less perfect IF(n=0) crystals. The transformation from NIF to IF crystals needs a prolonged time (after more than a week). For the TPEO-(MW=3000) fraction, annealing behavior of the crystal shows a rate between the HPEO and PPEO fractions.[34]

Nonintegral and Integral Folding Chain Crystal Formations. SAXS experiments were performed to investigate the long period in these fractions. Parts a–d of Figure 11 illustrate four PEO(MW=3000) fractions having different end groups crystallized at 43 °C. For HPEO and MPEO fractions (Figure 11a,b), a single scattering maximum indicating the long period of 13.6 and 14.0 nm, respectively, is identified initially in a short

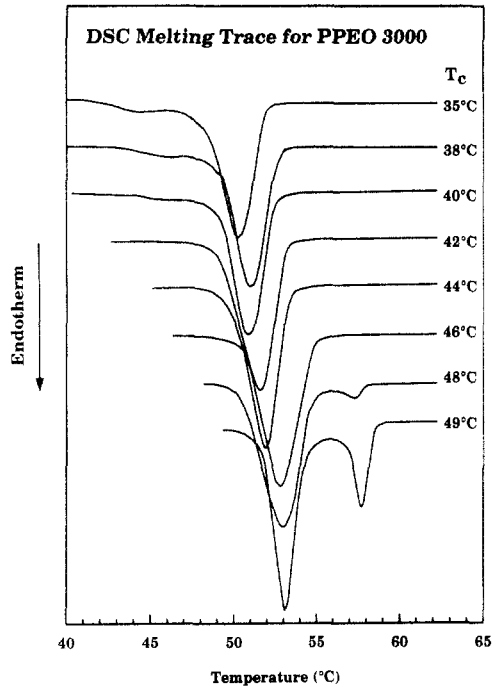

Figure 7. DSC endothermic melting curves for the PPEO-(MW=3000) fraction crystallized at different temperatures.

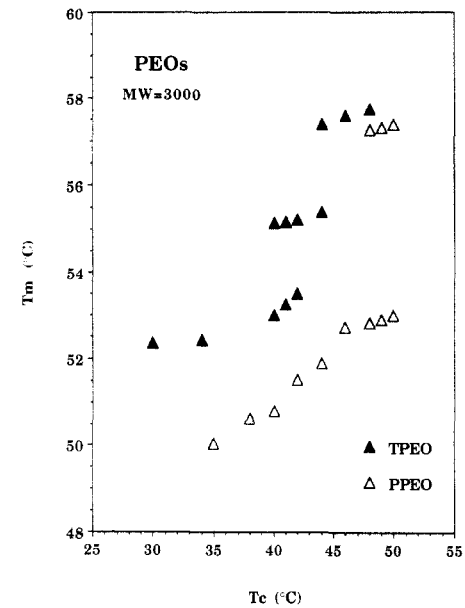

Figure 8. Relationships between T_m and T_c for TPEO and PPEO fractions with MW = 3000.

time period. With increasing crystallization time, this scattering peak decreases its intensity and converts into two new scattering peaks. At longer isothermal time [15 min for MPEO(MW=3000) and 45 min (not shown in the figure) for HPEO(MW=3000)], the initial scattering maximum totally vanished, leaving behind two new peaks with a larger peak at a higher s value (or a lower long spacing). These two scattering peaks correspond to the long period of 19.3 and 10.0 nm for HPEO(MW=3000) fractions and 20.0 and 10.3 nm for MPEO(MW=3000) fractions, respectively. They are representative of the integral folding chain (IF) crystals containing extended chain ($n = 0$) and once-folded chain ($n = 1$) conformations. At the same crystallization temperature, Figure 11c illustrates the SAXS patterns for the PPEO(MW=3000) fraction. It is seen that this fraction only shows one scattering maximum at a long period of 12.7 nm. The single scattering maximum does not convert into two peaks within the experimental time period (continuous scans

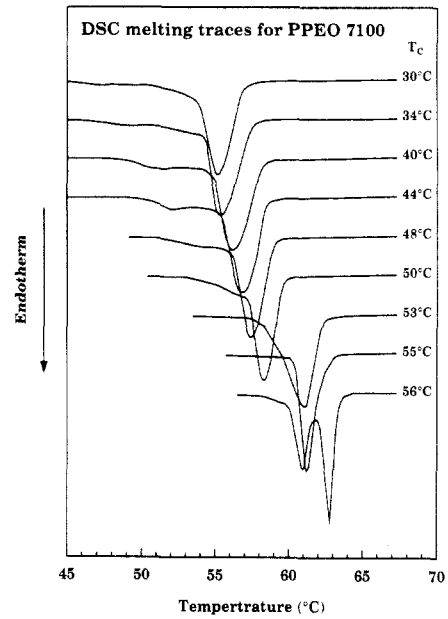

Figure 9. DSC endothermic melting curves for the PPEO-(MW=7100) fraction crystallized at different temperatures.

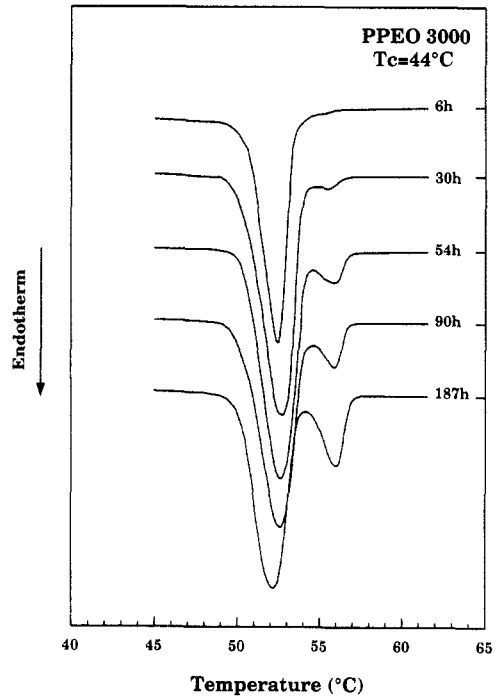

Figure 10. DSC endothermic melting traces for the PPEO-(MW=3000) fraction isothermally crystallized at 44 °C for different times.

were carried out in 45 min). This indicates that, during the crystallization, the long periods for this fraction remain almost constant. Nevertheless, IF crystals can still be observed after a prolonged isothermal time, such as the 300-h scan in Figure 11c. When the time is over 300 h for PPEO(MW=3000), and SAXS pattern shows that the majority of the scattering intensity has shifted to a long period of 20.5 nm, which represents the IF(n=0) crystal. Only a scattering shoulder corresponding to a long period of 12.7 nm remains. A minor scattering peak indicating a 10.6-nm-long period also appears which may represent the IF(n=1) crystal. [This peak may also be attributed to the second-order scattering of the 20.5-nm peak. Nevertheless, the peak intensity changes independently with crystallization time compared to that of the 20.5-nm peak, indicating that at least this scattering peak is partially formed due to the formation of the IF(n=1) crystal.] For

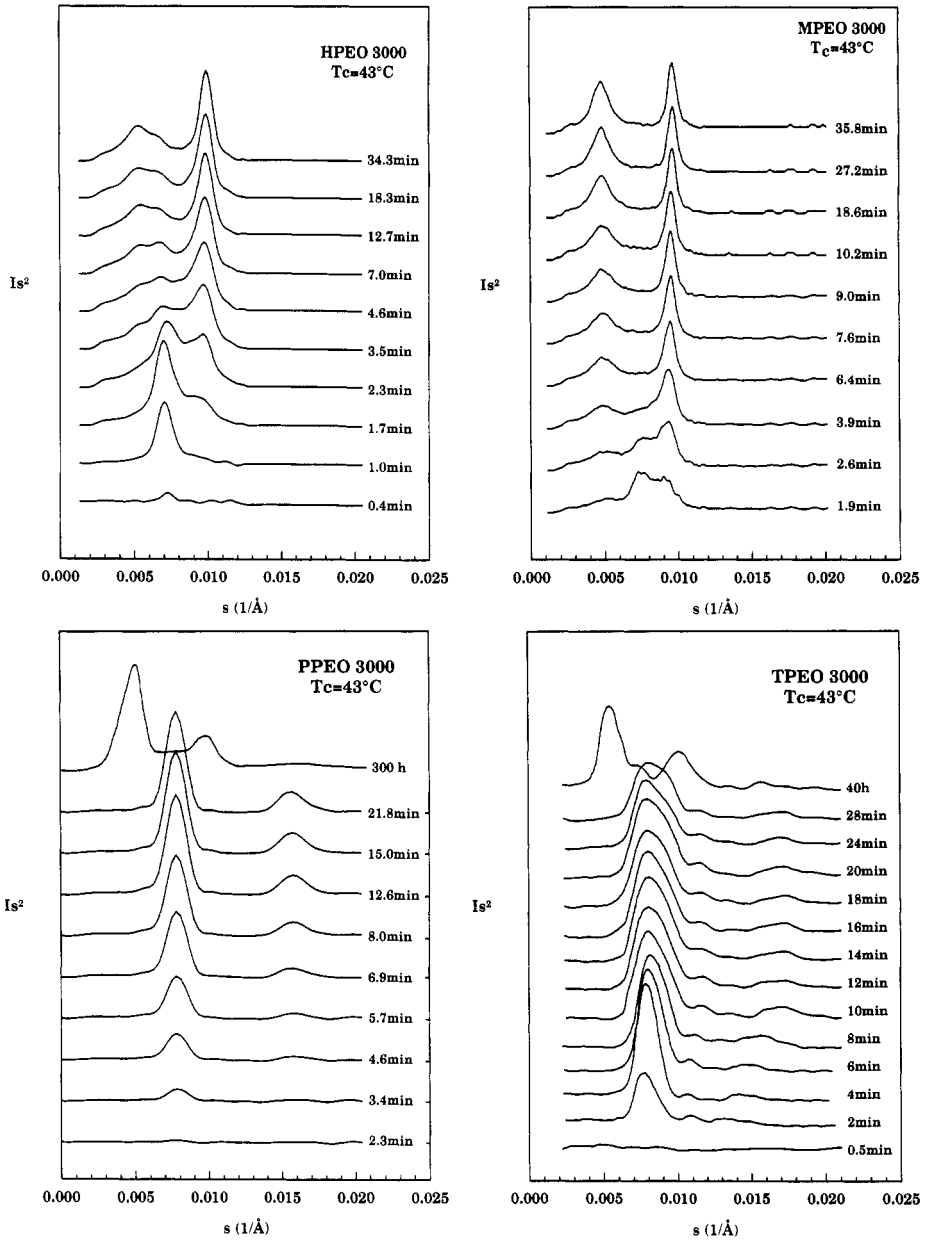

Figure 11. Synchrotron SAXS patterns for four PEO(MW=3000) fractions with the same molecular weight but different end groups crystallized at 43 °C; (a) hydroxy end groups; (b) methoxy end groups; (c) phenoxy end groups; (d) *tert*-butoxy end groups.

the TPEO(MW=3000) fraction, Figure 11d shows a case which is between those of the HPEO and PPEO fractions. Initially, a scattering peak appears at 13.0 nm. Within the experimental time period, changes of the scattering peak position can be seen by the first broadening this peak, and then forming new peaks with long periods of 20.3 and 10.5 nm at a prolonged time of 40 h. Both new peaks are representative of the IF(n=0) and IF(n=1) crystals of this fraction, with the majority of IF(n=0) crystals depending upon the annealing time. Compared to the HPEO and MPEO fractions with the same molecular weight (Figure 11a,b), the isothermal thickening and thinning rates in the PPEO fraction are much slower.

Parts a–c of Figure 12 are the SAXS patterns of three PEO(MW=7100) fractions with hydroxy, methoxy, and phenoxy end groups crystallized at 50 °C. Their IF crystals in these fractions are complicated since not only are IF(n=0) and IF(n=1) crystals present but also other IF crystals can form. As a result, multiple scattering peaks were observed. For example, Figure 12b shows that an initial scattering maximum of 18.6 nm appears in the MPEO(MW=7100) fraction. An additional peak develops at a long period of 23.9 nm in a later time, and it corresponds to the IF(n=1) crystal. Other scattering peaks correspond to the long periods of IF(n=3) and IF(n=4) crystals and/or high-ordering scattering. A similar observation can also be found in the case of the HPEO(MW=7100) fraction (Figure 12a). In contrast, in Figure 12c for the PPEO fraction, the scattering peak is almost a constant during the experimental time period. Further increasing the isothermal time up to 300 h leads to a new scattering peak developed at around 24.5 nm, which should represent the IF(n=1) crystal. However, the transformation from NIF to IF crystals even at such prolonged time is still far from completed.

Another important observation for these PEO fractions is that the long period of the initial NIF crystal increases with increasing isothermal crystallization temperature. For example, a long period of 13.0 nm is found in the HPEO(MW=3000) fraction at T_c = 39 °C, which increases to 15.4 nm at T_c = 47 °C; for the PPEO(MW=3000) fraction, the initial long spacing at T_c = 38 °C is 12.0 nm which increases to 14.0 nm at T_c = 45 °C. A similar observation was also seen in the PEO(MW=7100) fractions. The differences in the long periods among the PEO fractions with different end groups decrease with increasing the

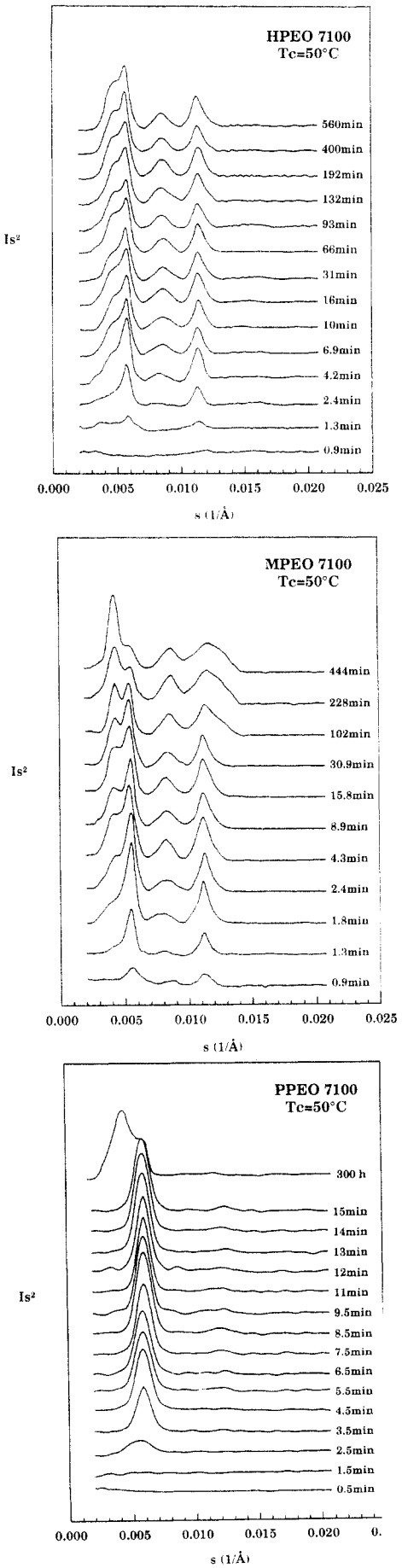

Figure 12. Synchrotron SAXS patterns for three PEO(MW=7100) fractions with the same molecular weight but different end groups crystallized at 45 °C: (a) hydroxy end groups; (b) methoxy end groups; (c) phenoxy end groups.

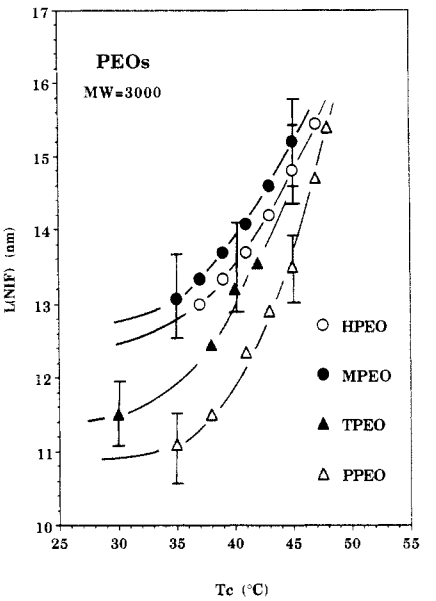

Figure 13. Relationships between the long period and crystallization temperature for four PEO(MW=3000) fractions.

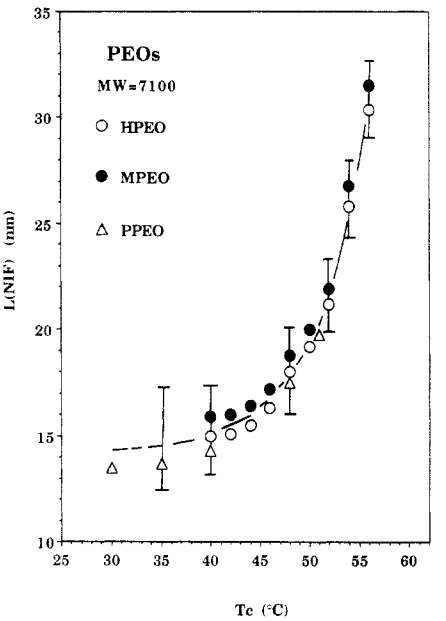

Figure 14. Relationships between the long period and crystallization temperature for three PEO(MW=7100) fractions.

crystallization temperature as well as the molecular weight. These results are shown in Figures 13 and 14. The vertical bars are the TEM results of the long periods for different fractions (the long periods of IF crystals are not shown in these figures). It is evident that both SAXS and TEM data agree well with each other. Figure 15 is a typical TEM morphological photograph of the HPEO(MW=7100) fraction crystallized at 50 °C.

Linear Crystal Growth Rates of PEO Fractions. Figure 16 shows the linear crystal growth rate data for four PEO(MW=3000) fractions at different crystallization temperatures. These data were measured from the spherulitic and/or hedritic growths using PLM. It is seen that the MPEO(MW=3000) fraction shows the fastest crystal growth rate, followed by HPEO, TPEO, and finally PPEO(MW=3000) fractions. These growth rate curves can be vertically and horizontally shifted and superimposed into a master curve. Using the MPEO(MW=3000) fraction as a reference, the vertical shift factors are about 3 times the growth rate (G) for the HPEO fraction, 0.5 order of magnitude for the TPEO fraction, and close to

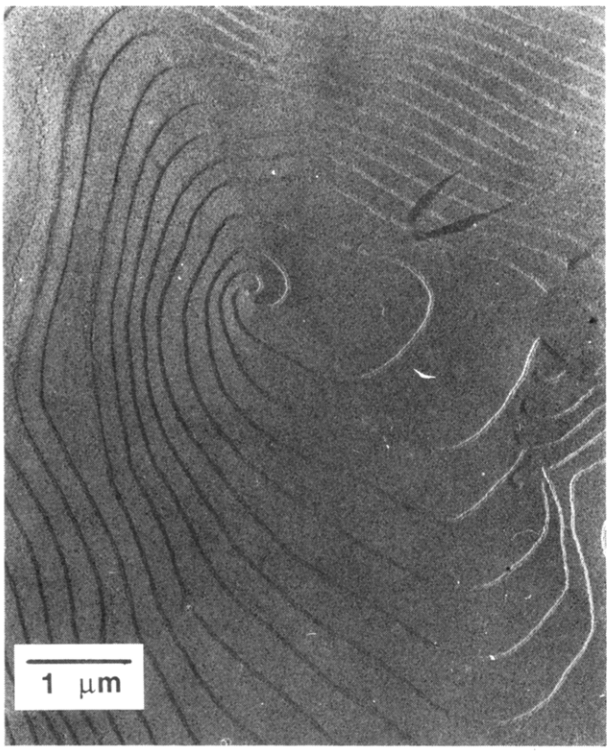

Figure 15. Typical TEM morphological photograph of the HPEO(MW=7100) fraction crystallized at 50 °C.

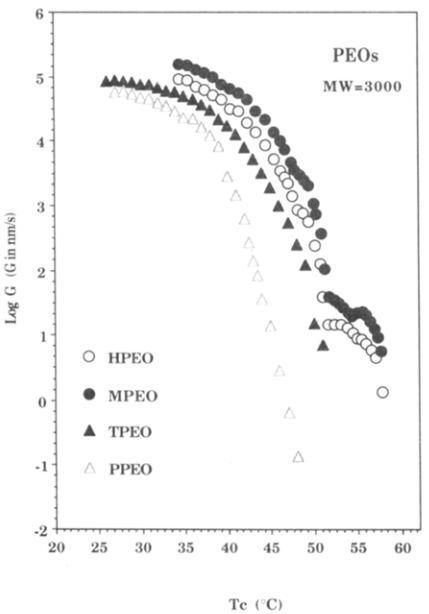

Figure 16. Linear crystal growth rate data of four PEO-(MW=3000) fractions measured through their spherulitic and hedritic growths at different crystallization temperatures.

1 order of magnitude for the PPEO fraction. The horizontal shift factors are about 3, 5, and 9 °C for these fractions, correspondingly. When the molecular weight increases to 7100, the differences in the crystal growth rates for these features are substantially reduced. For example, the crystal growth rates of the HPEO(MW=7100) and MPEO(MW=7100) fractions are almost identical;[34] the PPEO(MW=7100) fraction needs very little vertical shift in the growth rate and a horizontal shift factor of 4 °C if one uses the growth rates of the HPEO and MPEO fractions as references. The data are shown in Figure 17. It seems that both vertical and horizontal shift factors decrease with reduction not only in the size of the end groups but also the molecular weight.

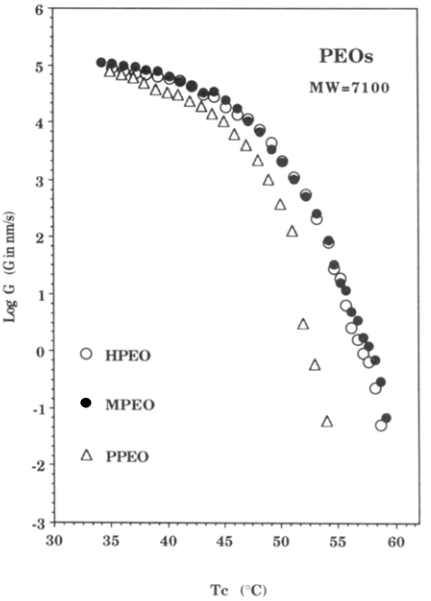

Figure 17. Linear crystal growth rate data of three PEO-(MW=7100) fractions measured through their spherulitic and hedritic growths at different crystallization temperatures.

Discussion

The physical meaning of the experimentally observed long period in the low molecular weight PEO fractions should be first described. A generally accepted definition of the long period obtained from SAXS experiments in a semicrystalline polymer system is the average distance between the center of gravity of two adjacent lamellae. In this case interfaces between crystalline and amorphous regions are also included in the long period. For the HPEO and MPEO fractions, we have assumed that the long period observed from the IF crystals is an approximate representation of the fold length of the lamellar crystal. In Figure 3, the degrees of crystallinity of these fractions with a molecular weight of 3000 are high. For the HPEO and MPEO fractions, the degree crystallinity are over 95%. For the TPEO and PPEO fractions, the degrees of crystallinity are above 90%. It should be noted that the end groups are about 3.8% and 5% of the total weight percentage, respectively, due to the relatively heavy end groups and high end-group densities. This leads to an even higher percentage of the crystallinity contributed by pure ethyleneoxy units in these PEO fractions. These high degrees of crystallinity indicate that the long period is near the lamellar thickness. It should be noted that these PEO fractions are not exactly monodisperse. The fold lengths of IF crystals are thus slightly fluctuated, and the SAXS data only provide average values. It is possible that a very small amount of ethyleneoxy units is not crystallized and remained on the lamellar surfaces. Furthermore, although the end groups do not take part in the IF crystal lattice and they are rejected onto the IF lamellar crystal surfaces, the end groups would still occupy space. The long periods of the PPEO and TPEO fraction should thus be thicker than the other two fractions (HPEO and MPEO). This expectation agrees well with our experimental results. For example, the length of a phenoxy group is approximately 0.5–0.6 nm. Two end groups for each chain make an increase of 1.0–1.2 nm for the long period of IF(n=0) crystals in the PPEO fraction. This is consistent with a difference in the long periods of 1.3 nm found when comparing the long period of IF(n=0) crystals for the PPEO(MW=3000) fraction with that of the HPEO-(MW=3000) fraction. In the IF(n=1) crystals, the long

period depends upon the packing of the end groups. The end groups may either concentrate on one side of the lamellar surface or be randomly distributed on both surfaces. At least, a 0.5–0.6-nm difference should be observed in the long periods between the PPEO and HPEO fractions with once-fold chains. Experimental data show a 0.6-nm difference in the IF(n=1) crystals between these two fractions with MW = 3000. For TPEO fractions, the length of a *tert*-butoxy end group is roughly 0.3–0.4 nm. The effect on the long period must be less than that in PPEO fractions, which has also been observed from experiments.

Regarding the NIF crystals, the long period can be understood through combining the experimental observations of the crystallization kinetics from DSC and WAXD measurements (Figures 5–10) and the SAXS results in Figures 11 and 12. For the MPEO and HPEO fractions, the long periods of the NIF crystals have been assumed to be the fold lengths of lamellar crystals due to their high degrees of crystallinity and small sizes of the end groups.[1-3] On the other hand, the crystallization process is not completed for the PPEO(MW=3000) fraction until t_c = 70 min and for the TPEO(MW=3000) fraction until t_c = 30 min at T_c = 43 °C (from DSC and WAXD). However, the scattering maximum (shown in Figure 11c) does not change in this period of time, but the scattering intensity continues to increase. This reveals that, for the PPEO(MW=3000) fraction during the crystallization, the NIF lamellar crystals develop a crystalline domain (most likely, spherulites and/or hedrites[32] in the melt, where no substantial change of the long period is expected in the initial period of time. It is conceivable that within the crystal domain only one type of lamellar thickness initially forms and can be continuously developed in size. The transformation from NIF to IF crystals takes a much longer time to accomplish than the development of crystallinity (Figure 11c). This assumption has been confirmed via TEM observations.[35] The crystallization, thickening, and thinning behaviors of the TPEO(MW= 3000) fraction are between the cases of the PPEO and HPEO fractions. For both the PPEO and TPEO fractions, the maximum degrees of crystallinity (by weight) are above 90%, since roughly more than 85% of the maximum crystallinity has been approached after NIF crystallization (Figure 10). This difference may be attributed to the end groups within the crystals and/or a small fraction of the chain segments in the amorphous region due to folds, long loops, and cilia. Transformation from NIF to IF crystals shows a small increase (less than 10%) in the crystallinity determined by DSC and WAXD. As a result, the long periods for both PPEO and TPEO fractions observed through SAXS were only approximate (perhaps, above 90% accuracy) to the fold lengths of NIF lamellar crystals.

Moreover, it is interesting to observe that the widths of half-height of the scattering peaks observed in Figure 11 are in the range of 0.0005 (rad) and 0.002 (rad). Using the Scherrer equation, one can obtain an apparent size of the crystal (a lamellar correlation length) which is approximately 70–300 nm. This distance corresponds to about 5–20 layers of lamellar crystals. Generally speaking, MPEO and HPEO fractions show longer correlation lengths compared with those of TPEO and PPEO fractions.

Since our study focuses on the crystallization behavior of PEO fractions from the melt, it is important to understand the hydrogen-bonding effect of the HPEO fractions in the melt state. This has been accomplished by using measurements of different melt viscosities for both HPEO and MPEO fractions with a MW = 3000 as reported previously.[25] It is found that the hydrogen-bonding and O–H stretching bands are recognizable in the melt (Figure 2). Consequently, the apparent molecular weight of the HPEO(MW=3000) fraction is higher than other fractions in the melt due to the hydrogen bonding. In contrast, the fractions of MPEO, TPEO, and PPEO with a MW = 3000 only illustrated a pure end-group size dependence of the diffusional motion. This is seen in parts a and b of Figure 4. It should be noted that the self-diffusion coefficient is molecular weight and temperature dependent.[29] However, the activation energies of four different fractions do not change much. The self-diffusion coefficients of three PEO(MW=7100) fractions, on the other hand, do not differ as much as those of the PEO-(MW=3000) fractions. This can be explained by the decrease in the end-group density with increasing molecular weight. Furthermore, the molecular weight of 7100 approaches the molecular weight which starts introducing chain entanglement. In particular, HPEO and PPEO fractions with a MW = 7100 exhibit very closed self-diffusion coefficients. Apparently, this indicates that the hydrogen-bonding effect in the HPEO fraction to the diffusional motion is almost equivalent to the size effect of phenoxy end groups in the PPEO fraction under the condition of the same molecular weight (the same end-group densities).

During the crystallization (Figures 3 and 6), it is clear that the crystal structure of PEO fractions with different end groups does not change. Upon melting, the PPEO-(MW=3000) fracton shows one major endothermic peak that is undercooling dependent at low crystallization temperatures. This melting peak can be attributed to the NIF crystal melting, based on SAXS results. The SAXS peak positions in these fractions are at different s values as of IF crystals. In the low undercooling region, a high-temperature endothermic peak is attributed to the IF-(n=0) crystal melting. The transformation of NIF to IF crystals in the TPEO(MW=3000) fraction is not as slow as that of the PPEO(MW=3000) fraction. For IF(n=1) crystals, both PPEO and TPEO fractions only show minor contributions. The melting behavior of the MPEO-(MW=7100) fraction is similar to the case of HPEO-(MW=7100),[2] while that the PPEO(MW=7100) is simpler than its counterparts (Figure 9). This is because the NIF crystals in PPEO(MW=7100) are more kinetically stable than the other two cases, which are more difficult to be transferred into the IF crystals.

In regard to the NIF crystallization, two aspects are of particular interest to us. First, due to the same molecular weight and molecular weight distribution in the chosen fractions, any crystallization discrepancy can be attributed to the end-group effect, either by hydrogen bonding or size difference. Second, by increasing the molecular weight to approach the critical molecular weight of entanglement in PEO fractions, the end-group dependence on the crystallization behavior should decrease. This would indicate that the entanglement effect in the crystallization process is a more important factor compared to the end-group effect. From Figures 11 and 12, we find that the fold lengths of NIF crystals in different PEO fractions are not the same at the same crystallization temperature (undercooling differences are within 1.5 °C). The fold length decreases with the increasing end-group size, which shows the order of MPEO > HPEO > TPEO > PPEO at the same T_c. Furthermore, the fold length increases with increasing crystallization temperature (or decreasing undercooling) for every fraction (Figures 13 and 14). This seems to manifest that the NIF crystallization behavior

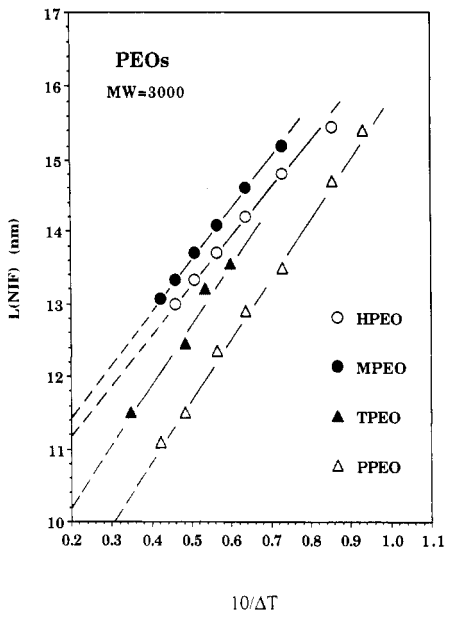

Figure 18. Relationships between fold lengths and reciprocal undercoolings for four PEO(MW=3000) fractions with different end groups.

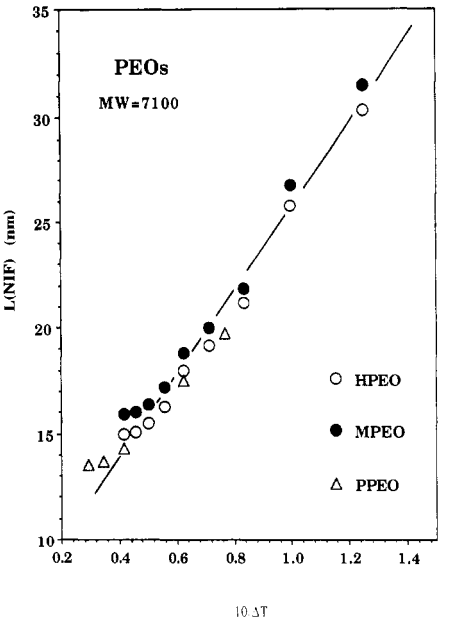

Figure 19. Relationships between fold lengths and reciprocal undercoolings for three PEO(MW=7100) fractions with different end groups.

can be described by conventional nucleation theory.[32] If one plots the data using the fold length versus the reciprocal undercooling, a linear relationship can be found. This indicates that NIF crystals in these fractions behave similarly to the folded chain polymer crystals,[36-39] disregarding the differences of the end groups. The relationships of the fold length and the reciprocal undercooling are illustrated in Figure 18 for four fractions with a molecular weight of 3000. On the basis of the nucleation theory,[40-44] the slope of this relationship represents the value of $2\sigma_e T_m/\Delta h_f$, where σ_e is the fold or end surface free energy, Δh_f and T_m are the heat of fusion and melting temperature; and the intersection represents the value of $kT/b_0\sigma$, where k is Boltzmann's constant, b_0 is the thickness of one chain monolayer along the crystal growth direction, and σ is the lateral surface free energy. From Figure 18, we find that the value of σ_e PPEO(MW=3000) fraction (which possesses the highest σ_e value) is about 1.3 times higher than the HPEO(MW=3000) fraction, while the other two are in between these cases. It should be noted that the precise T_m and Δh_f for NIF crystals are not well established, and, therefore, only relative ratios are provided here instead of the absolute values. Moreover, the values of σ for these fractions show a 1.5 times difference with changing from PPEO(MW=3000) (which possesses the highest σ value) to MPEO(MW=3000) (which possesses the lowest σ value) fractions. In Figure 19 the relationships between the fold length and reciprocal undercooling for three PEO(MW=7100) fractions are also plotted. Using the same theoretical treatment, we find that both values of σ_e and σ show very little difference among MPEO, HPEO, and PPEO fractions. It is evident that the difference of the fold lengths among the three PEO(MW=7100) fractions within the experimental error although a rough tendency can still be observed. At the same crystallization temperature (or approximately the same undercooling) the sequence of fold lengths is MPEO, followed by HPEO, and PPEO which shows the shortest fold length. Again, this indicates that the end group reduces its influence to the crystallization behavior when the end-group density is decreased and chain entanglement is introduced.

The microscopic mechanism of such a decrease in the fold length in relation to the size of the end groups may involve both nucleation and crystal growth of chain molecules from the melt to the growing surface. In the low molecular weight PEO fractions, the end-group density is high, which always affects the molecular diffusion in the melt (Figure 4a,b). However, as long as the crystal growth is nucleation controlled with the same diffusional activation energy, the diffusion process is not a rate-determining step for the crystallization. For HPEO fractions, it has been recognized that hydrogen bonding in the melt leads to an increase of apparent molecular weight. Since it is known that, in a molecular weight region below 20 000 in PEO fractions, linear crystal growth rates are clearly molecular weight dependent,[12,45] this may cause the decrease of linear crystal growth rates in HPEO fractions compared with those in MPEOs.[25] However, in the cases of MPEO, TPEO, and PPEO fractions this reason cannot be invoked since no hydrogen bonding exists in the fractions (Figure 1). An alternative explanation is that when a chain molecule is absorbed onto the growing surface, the end groups may locate on the surface and form surface defects due to their large volumes and noncrystallizable geometry. This surface thus possesses a higher entropy compared to the normal crystal growing surface without defects.[46,47] The distribution of these defects along the direction of chain molecules in the lamellar crystal may not be random. Instead, the defects may aggregate near the surfaces of the lamellar crystals. It is known that the fold length of a surface nucleation and crystal growth is determined through two opposite factors: the nucleation barrier and the driving force for crystal growth after the nucleation.[47] The former increases with the fold length and slows down the nucleation rate, and the latter enhances the growth rate with an increasing fold length. A high-entropy surface, perhaps, contributes an additional term to the nucleation barrier which may be combined with the lateral surface free energy term. Therefore, this will lead to a shift of the fold length toward an even lower value due to the bulky end groups, which is consistent with our results as shown in Figures 16 and 17. Only after the bulky end groups are rejected or diffused to certain local sites that have lower energy can the crystal grow further spread. Since the diffusional motion of the defects is temperature-dependent, one expects that the fold length should be less differed from the end groups at

high crystallization temperatures. This is what has been observed in Figures 13 and 14.

From this microscopic description, one may also try to explain the end-group dependence of the thickening and the thinning processes during the transformation from NIF to IF crystals in the PEO fractions. Since these processes usually take place after the crystallization in the undercooling region studied, it is logical that a chain sliding diffusional motion along the c-axis in the crystal containing a bulkier end group becomes increasingly difficult due to the large volume and higher friction coefficient of the motion. This kind of motion should be similar to the chain extension in polyethylene crystals under elevated pressure.[48-50] The rates of these processes in PPEO fractions are 2–3 orders of magnitude slower than those in their counterparts of MPEO fractions. Furthermore, it seems that, as end groups become bulkier, less IF(n=1) crystals may form. In this case, the NIF crystal seems to prefer thickening over thinning. This should be associated with the chain conformations in the initial deposition process on growth surfaces and the later annealing process. During chain deposition, bulky end groups may place onto the growth surface, and thickening may lead them toward two opposite sides of the lamella to avoid a local-density increase and/or surface packing difficulties. This is perhaps the reason why in both PPEO(MW=3000) and TPEO(MW=3000) fractions only a minor amount of IF(n=1) crystals can be experimentally found in SAXS results (Figure 11c,d).

It is interesting to note the disappearance of the end-group dependence with increasing molecular weight during crystallization and crystal melting behavior. Since the end-group density decreases with increasing molecular weight, fewer defects may form on the crystal growth surface. One may expect that entropy of the growing surface is not high enough to substantially decrease the fold length. In the cases of the MPEO and PPEO fractions with a MW = 7100, their linear crystal growth rates are thus less affected compared to their counterparts of PEO(MW=3000) fractions. When examining these fractions, it is important to recognize the chain entanglement effect. We believe the chain entanglement effect has a greater impact on crystallization than the end-group factor after the chain length exceeds the critical molecular weight of entanglement. In other words, polymer crystallization is a disentanglement process providing that the chain molecules have a chance to rearrange themselves during crystallization.

Conclusion

We have demonstrated the end-group dependence on crystallization and crystal melting behavior of a series of low molecular weight PEO fractions. All fractions exhibit a NIF crystal at their initial, transient state during crystallization. The kinetic stability of this NIF crystal is largely dependent upon the size of the end group. By increasing the size of the end group, not only does the transformation of the NIF to IF crystals become increasingly difficult but also the linear crystal growth is hampered even with the same molecular weight and molecular weight distribution. The former process occurs in the direction perpendicular to the lamellar crystal surface, while the latter is in the direction normal to the growing surface. The fold length of NIF crystals for each PEO fraction increases continuously with decreasing undercooling, similar to conventional folded-chain lamellar crystals observed in isothermal experiments. Moreover, the initial fold lengths of the NIF crystals are also end-group dependent. The bulkier end group leads to a decrease of the fold length, which was explained by the argument of a high-entropy growing surface due to the defect arrangements in a nucleation-controlled crystal growth. The NIF to IF crystal transformation can be observed through both thickening and thinning processes in PEO(MW=3000) fractions. Nevertheless, these processes are also end-group dependent. The PPEO(MW=3000) fraction shows a 2–3 order of magnitude slower transformation kinetics. The chain sliding diffusional motion along the c-axis in the crystals is expected to explain the experimental observations. The population of IF(n=1) crystals also decreases with increasing the size of the end groups. These processes are observed in both HPEO and MPEO fractions with MW = 7100 but severely hampered in the PPEO(MW=7100) fraction.

Acknowledgment. This work was supported by S.Z.D.C.'s Presidential Young Investigator Award from the National Science Foundation (DMR-9175538) and Exxon Education Foundation for the industrial matching funding. Research (in part) at the National Synchrotron Light Source (NSLS), Brookhaven National Laboratories, which is supported by the U.S. Department of Energy, Division of Materials Sciences and Division of Chemical Sciences. The study of MPEO fraction crystallization behavior was initially proposed by Professor J. D. Hoffman. His useful suggestions are also gratefully acknowledged.

References and Notes

(1) Cheng, S. Z. D.; Zhang, A.-Q.; Barley, J. S.; Chen, J.-H.; Habenschuss, A.; Zschack, P. R. *Macromolecules* **1991**, *24*, 3937.
(2) Cheng, S. Z. D.; Chen, J.-H.; Zhang, A.-Q.; Barley, J. S.; Habenschuss, A.; Zschack, P. R. *Polymer* **1992**, *33*, 1140.
(3) Cheng, S. Z. D.; Chen, J.-H.; Barley, J. S.; Zhang, A.-Q.; Habenschuss, A.; Zschack, P. R. *Macromolecules* **1992**, *25*, 1453.
(4) Ungar, G.; Keller, A. *Polymer* **1986**, *27*, 1835.
(5) Ungar, G.; Keller, A. *Polymer* **1987**, *28*, 1899.
(6) Organ, S. J.; Ungar, G.; Keller, A. *Macromolecules* **1989**, *22*, 1995.
(7) Arlie, J. P.; Spegt, P. A.; Skoulios, A. E. *Makromol. Chem.* **1966**, *99*, 170.
(8) Arlie, J. P.; Spegt, P. A.; Skoulios, A. E. *Makromol. Chem.* **1967**, *104*, 212.
(9) Spegt, P. *Makromol. Chem.* **1970**, *139*, 139.
(10) Kovacs, A. J.; Gonthier, A. *Colloid Polym. Sci.* **1972**, *250*, 530.
(11) Kovacs, A. J.; Gonthier, A.; Straupe, C. *J. Polym. Sci., Polym. Symp.* **1975**, *50*, 283.
(12) Kovacs, A. J.; Straupe, C.; Gonthier, A. *J. Polym. Sci., Polym. Symp.* **1977**, *59*, 31.
(13) Kovacs, A. J.; Straupe, C. *J. Cryst. Growth* **1980**, *48*, 210.
(14) Kovacs, A. J.; Straupe, C. *Faraday Discuss. Chem. Soc.* **1979**, *68*, 225.
(15) Buckley, C. P.; Kovacs, A. *Kolloid Z. Z. Polym.* **1976**, *254*, 695.
(16) Buckley, C. P.; Kovacs, A. *Progr. Colloid Polym. Sci.* **1975**, *58*, 44.
(17) Hartly, A.; Leung, Y. K.; Booth, C.; Shepherd, I. W. *Polymer* **1976**, *17*, 354.
(18) Fraser, M. J.; Marshall, A.; Booth, C. *Polymer* **1977**, *18*, 93.
(19) Ashman, P. C.; Booth, C. *Polymer* **1973**, *14*, 300.
(20) Cooper, D. R.; Booth, C. *Polymer* **1977**, *18*, 164.
(21) Shimada, T.; Okui, N.; Kawai, T. *Makromol. Chem.* **1980**, *181*, 2643.
(22) Galin, J.-C.; Spegt, P.; Suzuki, S.; Skoulios, A. E. *Makromol. Chem.* **1974**, *175*, 991.
(23) Thierry, A.; Skoulios, A. E. *Colloid Polym. Sci.* **1977**, *255*, 334.
(24) Thierry, A.; Skoulios, A. E. *Eur. Polym. J.* **1977**, *13*, 169.
(25) Cheng, S. Z. D.; Chen, J.-J.; Zhang, A.-Q.; Heberer, D. P. *J. Polym. Sci., Polym. Phys. Ed.* **1991**, *29*, 299.
(26) Devos, R. J.; Goethals, E. J. *Makromol. Chem., Rapid Commun.* **1985**, *6*, 53.
(27) Devos, R. J.; Goethals, E. J. *Polym. Bull.* **1986**, *15*, 547.
(28) von Meerwall, E. D. *Adv. Polym. Sci.* **1983**, *54*, 1; *Rubber Chem. Technol.* **1985**, *58*, 527.

(29) Cheng, S. Z. D.; Barley, J. S.; von Meerwall, E. D. *J. Polym. Sci., Polym. Phys. Ed.* **1991**, *29*, 515.
(30) von Meerwall, E. D.; Palunas, P. *J. Polym. Sci., Polym. Phys. Ed.* **1987**, *25*, 1439.
(31) Ferry, J. D. *Viscoelastic Properties of Polymers*, 3rd ed.; Wiley: New York, 1980; p 136.
(32) Cheng, S. Z. D.; Chen, J.-H. *J. Polym. Sci., Polym. Phys. Ed.* **1991**, *29*, 311.
(33) Cheng, S. Z. D.; Zhang, A.-Q.; Chen, J.-H.; Heberer, D. P. *J. Polym. Sci., Polym. Phys. Ed.* **1991**, *29*, 287.
(34) Wu, S. S. Ph.D. Dissertation, Department of Polymer Science, The University of Akron, Akron, OH, 1994.
(35) Chen, J.-H.; Wu, S. S.; Cheng, S. Z. D., in preparation.
(36) Hoffman, J. D. *Macromolecules* **1986**, *19*, 1124.
(37) Buckley, C. P. *Polymer* **1980**, *19*, 444.
(38) Sadler, D. M. *J. Polym. Sci., Polym. Phys. Ed.* **1985**, *23*, 1533.
(39) Skoulios, A. E. *Kolloid Z. Z. Polym.* **1969**, *234*, 1059. See also: Gilg, P. B.; Skoulios, A. E. *Makromol. Chem.* **1971**, *140*, 149.
(40) Lauritzen, J. I., Jr.; Hoffman, J. D. *J. Appl. Phys.* **1973**, *44*, 4340.
(41) Hoffman, J. D.; Frolen, L. J.; Ross, G. S.; Lauritzen, J. I., Jr. *J. Res. Natl. Bur. Stand., Sect. A* **1967**, *71A*, 261.
(42) Hoffman, J. D.; Davis, G. T.; Lauritzen, J. I., Jr. In *Treatise on Solid State Chemistry*; Hannay, N. B., Ed.; Plenum: New York, 1976; Vol. 3, Chapter 7, pp 497–614.
(43) Hoffman, J. D. *Polymer* **1982**, *23*, 656; **1983**, *24*, 3.
(44) Hoffman, J. D.; Miller, R. L. *Macromolecules* **1988**, *21*, 3038.
(45) Cheng, S. Z. D.; Wunderlich, B. *J. Polym. Sci., Polym. Phys. Ed.* **1986**, *24*, 595.
(46) Hoffman, J. D. *Polymer* **1985**, *26*, 1763.
(47) Sadler, D. M. *Polymer* **1983**, *24*, 1401; **1987**, *28*, 1440.
(48) Wunderlich, B.; Melillo, L. *Makromol. Chem.* **1968**, *118*, 250.
(49) Hikosaka, M.; Tsukijima, K.; Rastogi, S.; Keller, A. *Polymer* **1992**, *33*, 2502.
(50) Hikosaka, M.; Rastogi, S.; Keller, A.; Kawabata, H. *J. Macromol. Sci., Phys.* **1992**, *B31* (*1*), 87.